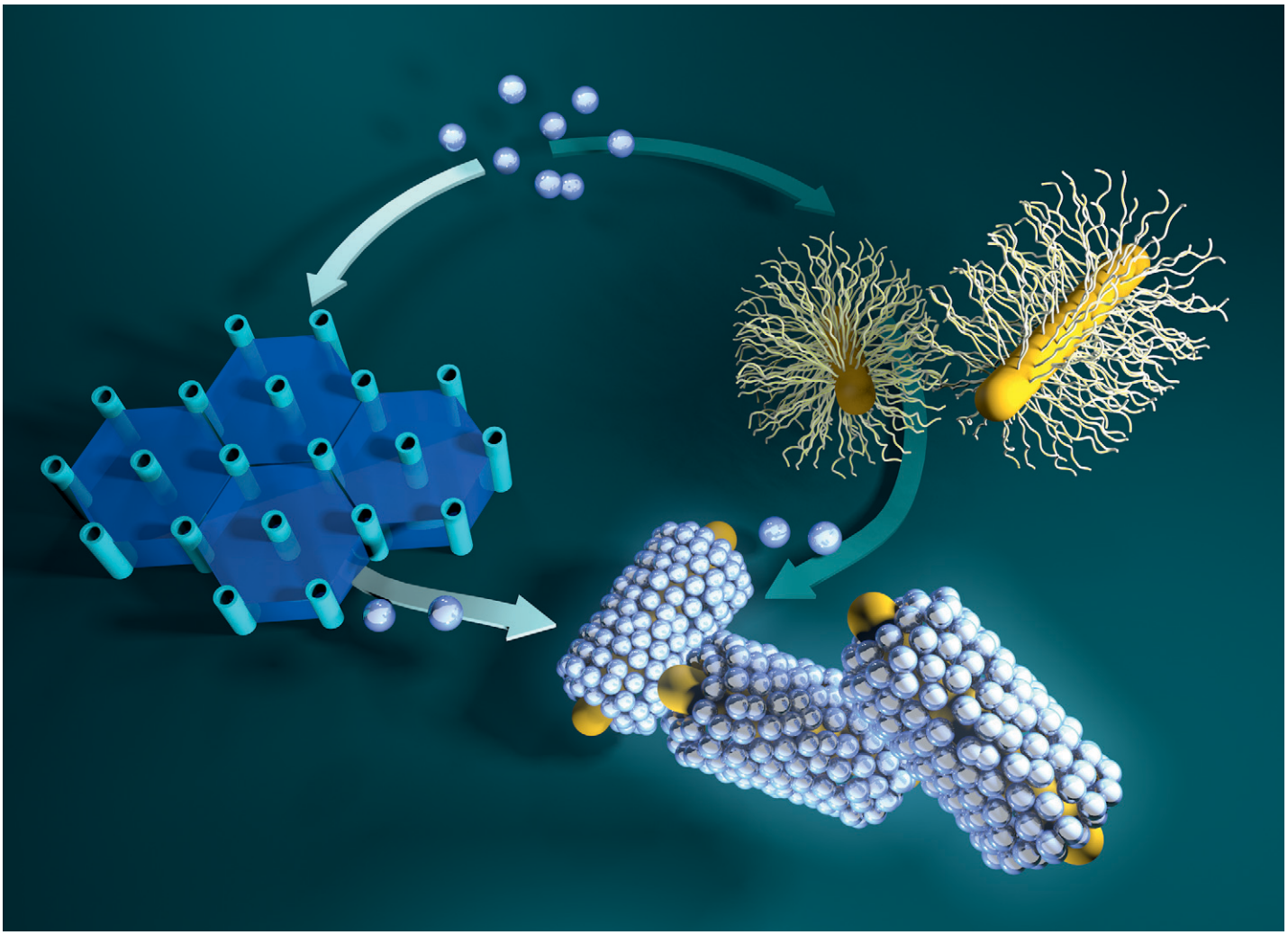

Research highlights of Josef Breu, Thomas Lunkenbein et al. from the Department of Chemistry and the Bavarian Polymer Institute at the University of Bayreuth and the Department of Inorganic Chemistry at the Fritz-Haber-Institut der Max-Planck-Gesellschaft, Berlin.

Electrostatic attraction of nanoobjects – a versatile strategy towards mesostructured transition metal compounds

Coulomb interaction between ionizable polymeric templates and oppositely charged oligo-ions allows for reliable synthesis of robust mesostructured compounds with tunable wall chemistry. The concept, examples, and limitations of this mesostructuring strategy are discussed and are compared to general approaches. Image reproduced by permission of Daniela Leitner.

As featured in:

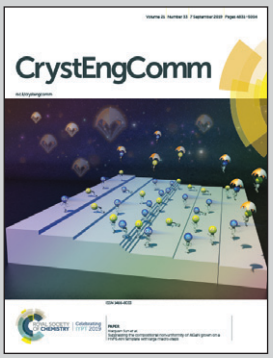

See Josef Breu, Thomas Lunkenbein *et al.*, *CrystEngComm*, 2019, **21**, 4840.

ROYAL SOCIETY OF CHEMISTRY | Celebrating IYPT 2019

rsc.li/crystengcomm

Registered charity number: 207890

CrystEngComm

HIGHLIGHT

View Article Online
View Journal | View Issue

Cite this: *CrystEngComm*, 2019, **21**, 4840

Electrostatic attraction of nanoobjects – a versatile strategy towards mesostructured transition metal compounds

Carina Bojer,[a] Kevin Ament,[a] Holger Schmalz,[a] Josef Breu *[a] and Thomas Lunkenbein *[b]

This highlight summarizes current challenges of mesostructuring and focuses on the scope and the potential of the ELAN – (electrostatic attraction of nanoobjects) strategy in mesostructuring of transition metal compounds. It discusses the limitations of this concept and highlights prominent examples. ELAN exploits the Coulomb attraction between inorganic precursors and polymeric templates in order to prevent macrophase separation. Essential requirements for ELAN are tailor-made, mesoscopic polyelectrolytic templates and charged molecular oligo-ions or stable colloids carrying a surface charge. The ELAN-strategy is highly reliable and opens the way to crystalline, mesoporous transition metal compounds with predefined polymorphism. It also provides the possibility to adjust wall chemistry and reactivity as well as the flexibility to synthesise different mesostructures (spheres, non-woven arrays or hexagonally ordered phases).

Received 17th February 2019,
Accepted 16th May 2019

DOI: 10.1039/c9ce00228f

rsc.li/crystengcomm

Introduction

Modern life would not be conceivable without the economic and efficient synthesis of functional base chemicals applying sophisticated catalysts. To meet the prospective demand on base chemicals needed in vital sectors, such as medicine, transport or nutrition, existing technologies have to be continuously improved or supplemented by new materials. In general, heterogeneous catalysis can be described as a multistep technology which involves reactant(s) diffusing and adsorbing to the active surface of a catalyst, the catalytic reaction itself, followed by desorption of the product(s) and dynamic surface regeneration of the catalyst.[1] Catalytic materials are often complex nanoparticular solids or supported systems, *i.e.* oxidic supports are decorated by metallic nanoparticles.[2–4] Nanoparticles exhibit modified morphologies and electronic structures at the surface and, as a result, different properties compared to their bulk analogues, which in combination enables high catalytic turnovers.[5–8] In addition, to assure accessibility to the active phase a high surface area is indispensable and usually goes along with some type of porosity that enhances proper mass transport.[9,10] Yet, efficient industrially relevant heterogeneous catalysts are empirically optimized systems, where further improvement of their performance, such as selectivity or life time enhancement, is difficult, if possible at all. These catalytic systems often have to resist harsh and reactive environments in catalytic reactors, which limits their life time.[11] In order to reduce deactivation phenomena induced by catalysis, like sintering, poisoning or conversion into thermodynamically more stable but inactive compounds, and, thus, to enhance life time of a catalytic system, materials with a high internal mass transport would be desirable.

Research on porous materials has gained world-wide attraction in the last decades.[12–14] In general, porous materials are classified as microporous (pore size <2 nm), mesoporous (2–50 nm) and macroporous (>50 nm) (Fig. 1).[15] Mesoporous materials can be considered as a fair compromise between maximising the catalytically active surface area while ensuring at the same time a high accessibility of the active phases.[16] The

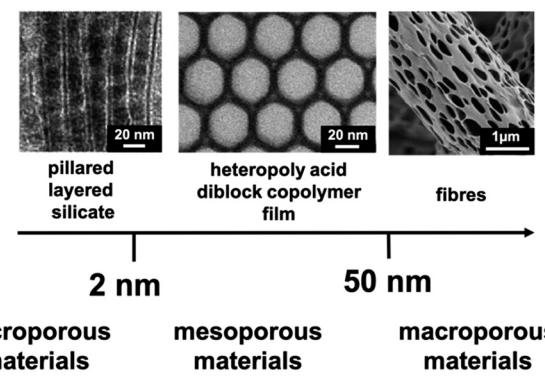

Fig. 1 Schematic representation of microporous, mesoporous and macroporous materials exemplified by electron microscopy (EM) images.

[a] *Department of Chemistry and Bavarian Polymer Institute, University of Bayreuth, Universitätsstr. 30, 95440 Bayreuth, Germany. E-mail: josef.breu@uni-bayreuth.de*
[b] *Fritz-Haber-Institut der Max-Planck-Gesellschaft, Department of Inorganic Chemistry, Faradayweg 4-6, 14195 Berlin, Germany. E-mail: lunkenbein@fhi-berlin.mpg.de*

large field of mesoporous materials and the synthesis strategies were recently reviewed by several groups.[11,12,17–19]

Mesoporous materials are synthesized utilizing both hard and soft templates. Hard templating, which is often referred to as nanocasting or exotemplating, requires a solid and porous support, which is replicated by impregnation with an inorganic precursor. After chemical removal of the template a negative copy is obtained. Examples for common hard templates are silica nanoparticles, zeolites, colloidal crystals, mesoporous silica or aluminium oxide membranes. The hard templating strategy promises high stability as well as reproducibility and is commonly used to prepare highly crystalline mesoporous metal oxides. However, it is expensive and limits the pore wall thickness to approximately 10 nm.[20–24]

The soft templating strategy takes advantage of surfactants as structure directing agents (SDAs), which comprise hydrophobic and hydrophilic moieties. Above the critical micelle concentration they form micellar nanostructures (*e.g.* spheres, rods) in solution that upon evaporation or addition of inorganic precursors self-assemble into one-, two- or three-dimensional (1D, 2D or 3D) supramolecular templates (cubic, hexagonal, layered, gyroid macrophases).[11,25–31] A more sophisticated branch of surfactants are amphiphilic block copolymers that are composed of solvophilic and solvophobic blocks.[32–34] Block copolymers offer a broad flexibility with respect to the dimensions of the generated mesophases by tailoring the molecular weight and composition of the employed block copolymers. In general, block copolymers can undergo microphase separation in the bulk forming mesoscale structures that consist of a core, which is surrounded by a corona. Throughout the manuscript we define side chains as the part of the block copolymer that is interacting with inorganic precursors and a polymeric brush denotes a rigid core-crosslinked template with ionizable side chains. A detailed description of polymeric brushes, their properties and application is beyond the scope of this highlight and can be found elsewhere.[35] Early successful examples of the soft templating approach are mesostructured materials such as MCM-41 or SBA-15.[36–38]

Clearly, to be able to address the great variety of different catalytic processes, each requiring its individual reaction conditions, a more general, versatile and robust approach for the preparation of mesoporous catalysts is needed. The new concept, moreover, ought to yield materials with pronounced stability of walls against changes in crystallinity, polymorphism and chemical nature induced by the catalytic reaction. Under the prevailing conditions of catalytic reactions dynamic chemical transformations should be suppressed that either lead to rapid deactivation or the destruction of the mesoporosity.

In this highlight, we will describe a new concept of mesostructuring which relies on the robust **el**ectrostatic **a**ttraction of **n**anoobjects (ELAN) and allows for enhancing mass transport within materials by means of mesostructuring. In brief, the ELAN strategy extents the concept of charged surfactants, such as cetyltrimethylammonium bromide (CTAB) that have been applied in early days of mesostructuring for biomedical and photocatalytic applications.[39–41] By this strategy chemically robust mesostructures may be assembled either from charged molecular or colloidal stable nanoparticular precursors in which the Coulomb interaction prevents macroscopic phase separation. These new materials can be applied as heterogeneous catalysts in solid–liquid or solid–gas catalysis. Furthermore, concepts are presented to adjust the chemical nature of the walls while preserving the mesostructure.

The mesostructuring challenge

Organic template directed synthesis of porous inorganic compounds like zeolites has long been transformed into a robust technical process.[42,43] Contrary to this, the utilization of supramolecular SDAs to assemble mesostructured inorganic materials with well-defined shape and pore size remains sophisticated and challenging. Their preparation strongly depends on the delicate interplay of micelle dynamics as well as the kinetics of hydrolysis and condensation of the inorganic precursor, which all need to happen on the same time scale to avoid macroscopic phase segregation. The kinetics depends crucially on the nature of the inorganic precursor and is influenced by minute changes in synthesis parameters, such as temperature, pH, concentration, solvent or ionic strength.[25,44,45] Means of independently and orthogonally controlling the individual steps are scarce. Many different recipes have been developed for the generation of various mesostructured materials by combining organic templates and inorganic precursors.[46] However, all of them require to strictly adhere to the complete set of the above-mentioned parameters.[25] Common inorganic precursors are hydrated silicic acids, metal salts, metal-oxo clusters or hydrolysable metal alkoxides (M–OR).[47–49] During initial hydrolysis reactive M–OH species are formed, which subsequently condense to form M–O–M or M–OH–M moieties.[19] Kinetic control over both hydrolysis and condensation is obtained by a careful adjustment of pH, concentration or the addition of small (stoichiometric) quantities of water. In this context, evaporation induced self-assembly (EISA) or trapping of preformed nano building blocks by suitable templates that hinder further condensation[47,50] are two smart self-regulating approaches. The EISA process relies on homogeneous solutions of both inorganic precursor and organic SDA. During solvent evaporation, *i.e.* upon gradually increasing the concentration, at some stage a liquid crystalline mesophase is formed, in which the inorganic precursor is embedded within the organic template.[50,51]

After succeeding in establishing the complex synthesis protocol, the job is not yet finished. Next, conditions need to be identified that allow for removal of the SDA from the initially obtained mesostructured hybrid material. Often, the desired application might require the crystallization of the initially amorphous walls and the control of the polymorphic structure. These post-synthetic (thermal) treatments may, however, cause the collapse of the mesostructure. The removal of the organic template while the mesoporosity is preserved is only possible, if concomitantly with the removal of

the SDA scaffold mechanically stable, self-supporting wall structures emerge. This requires a high inorganic loading within the final hybrid walls allowing for connecting individual building blocks *via* condensation.

Similarly, collapse of the mesostructure is often induced by density changes caused by crystallization of amorphous walls, polymorph transformations, or chemical reactions of the wall constituents.[51–53] In addition, sintering or vaporisation of volatile compounds at elevated temperature affect the wall thickness and may diminish the thermal stability of the final mesoporous compounds.[52]

Thermal template removal will consume oxygen and therefore will locally reduce oxygen fugacity, which in the beginning might then initiate reduction and at later stages reoxidation phenomena in the inorganic walls. Only redox insensitive compounds like silica or alumina remain unaffected.[51–53] All others will require some degree of control over oxygen fugacity during template removal.

Typically, template removal protocols are restricted to temperatures below 450 °C, which often leads to carbon or nitrogen residuals in the final mesoporous material.[44] In addition, the temperature is often too low to obtain fully crystalline mesostructured materials.[20,54] Although higher temperatures would lead to higher crystallinity, they promote the structural collapse due to the higher mobility of the atoms in the wall during crystallization.[44,54] To overcome this crystallization challenge, an additional carbonization step was introduced to temporarily line and stabilize the inorganic walls.[55–57] By subsequent carbon removal in oxidizing environments mesoporous and crystalline materials were obtained. The stabilizing carbon lining can either be added separately to the amorphous mesoporous compound or it can be formed *in situ via* pyrolysis of the polymeric entities inside the pores under inert gas atmosphere. The latter approach is often referred to as combined assembly by soft and hard chemistries (CASH) method.[55]

To overcome the above mentioned pitfalls towards mesostructured and mesoporous materials we follow a strategy that is based on the **el**ectrostatic **a**ttraction of **n**anoobjects (ELAN), which may easily be combined with the CASH method. Details of the ELAN-strategy are explained in the subsequent section.

The ELAN-strategy (electrostatic attraction of nanoobjects)

Scope

The ELAN-strategy exploits the Coulomb attraction between colloidally stable nanoparticles carrying a surface charge or oligo-ions of inorganic precursors and oppositely charged amphiphilic diblock copolymers. As opposed to weak dipolar and van-der-Waals interactions, as provided by the standard Pluronic based SDAs, the electrostatic attraction *via* strong Coulomb interactions between the organic template and the inorganic precursor efficiently prevents macroscopic phase separation. In addition, pre-synthesized surface-charged inorganic colloids or oligo-ions have a lower specific charge density as compared to individual ions and therefore provide a much higher loading with inorganic precursors in the hybrid material formed. And finally, both precursor types represent stable intermediates on the way to bulk oxides, which releases the need to strictly synchronize hydrolysis and condensation and thus simplifies the formation of mesostructured hybrid materials.

Potential

The ELAN-strategy features two routes (Scheme 1) toward mesostructured compounds. These routes reflect the distinct nature of the polymeric templates. They are based on the EISA approach (ROUTE 1 in Scheme 1), which allows for obtaining inverse hexagonal mesostructures, and on core-crosslinked 1D pre-synthesized templates (ROUTE 2 in Scheme 1), which exploits the ability of amphiphilic diblock copolymers to microphase separate in the bulk. Both approaches involve ionizable amphiphilic diblock copolymers in the mesostructuring process. Similar to surfactants amphiphilic diblock copolymers can form micellar structures in solution and undergo microphase separation into block A and block B-rich domains in the bulk.[58–60] The separation of the blocks in selective solvents leads to a multitude of self-assembled microstructures and depends on the degree of polymerization, the composition and the Flory–Huggins segmental interaction parameter.[61,62] Amphiphilic diblock copolymer templates guarantee access to a plethora of different morphologies with defined shape and size of a core and corona.[63,64] The latter relates to the wall thickness obtainable.

In ROUTE 1 the charged inorganic precursor directly interacts with the ionizable block of the amphiphilic diblock copolymer. The *in situ* generated inorganic/organic hybrid micelle is stabilized in solution by a larger solvophilic block. After solvent evaporation inverse hexagonally ordered hybrid

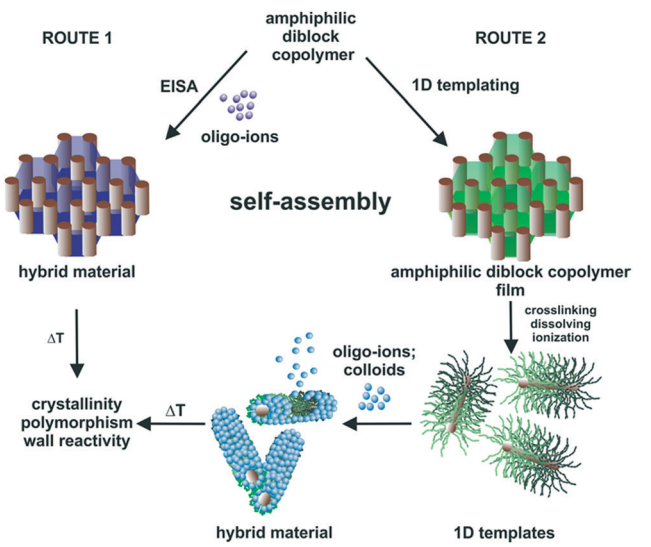

Scheme 1 The ELAN-strategy: alternative routes to obtain mesostructured functional materials by self-assembly of polyelectrolytic polymeric SDAs and inorganic precursors driven by Coulomb attraction.

materials are obtained that are composed of non-crosslinked polymeric cylinders embedded in an organic/inorganic hybrid. The observed mesophase depends on the loading of the inorganic precursor and the relative humidity. Subsequent thermal treatments in different atmospheres in principle would allow for template removal and the adjustment of crystallinity, polymorphism, as well as wall chemistry while the mesostructure is retained.

In ROUTE 2 microphase separation of the amphiphilic diblock copolymer upon slow solvent evaporation first leads to the formation of hexagonally ordered cylinders that are distributed in the polyelectrolytic matrix. The cylinders are then covalently cross linked allowing for subsequent dissolution by charging the corona. Rigid, highly charged 1D polyelectrolyte brushes are obtained that are accessible for the loading with oppositely charged inorganic precursors. The freezing of the dynamic nature of the micelles by core-crosslinking is crucial for this strategy since it allows for control of the template morphology and concomitant variation of reaction conditions. For example, when polybutadiene-*block*-poly(2-vinylpyridine) (PB-*b*-P2VP) with a PB content of 80 wt% is dissolved in tetrahydrofuran (THF), worm-like micelles are formed.[65] Changing the solvent would, however, trigger a structural transformation of the micelle and undesired template and mesostructure morphologies would be formed.[65]

A pre-requisite for a successful mesostructuring *via* this ELAN approach is the generation and preservation of charge at the amphiphilic diblock copolymer. The charge can be formed *in situ*, for instance, by protonation of nitrogen containing functional groups such as pyridines or amines with strong acids or by solution induced dissociation of polymeric acids, such as a sulfonic acid group. Strong acids like sulfonic acids are negatively charged over the entire pH range. In addition, permanent charges can also be introduced by post-synthetic quaternization of amino or pyridine groups. Amphiphilic diblock copolymers, which have been successfully used in the ELAN-approach are listed in Table 1.

Limitations

As outlined above the strategy is rather robust compared to other mesostructuring concepts. However, the applied

Table 1 Suitable amphiphilic diblock copolymers for the ELAN-strategy

Polymer	Abbreviation	Composition[a]	$Đ_M$[b]	Synthesis	Charge[c]	Source
Poly(styrenesulfonic acid)-*block*-poly(allyl methacrylate)	PSS-*b*-PAMA	M_n = 81 000 g mol^{-1} PSS = 69 wt% PAMA = 31 wt%	1.06	1. Sequential living anionic polymerization 2. Core-crosslinking 3. Sulfonation	pH independent (negative)	Ref. 68
Polybutadiene-*block*-poly(*N*,*N*-dimethylaminoethyl methacrylate)	PB-*b*-PDMAEMA	M_n = 29 000 g mol^{-1} PB = 78 wt% PDMAEMA = 22 wt%	1.03	1. Sequential living anionic polymerization	pK_a = 8.44	Ref. 69 Ref. 70
Polybutadiene-*block*-poly(2-vinylpyridine)	PB-*b*-P2VP^{30}	M_n = 30 000 g mol^{-1} PB = 74 wt% P2VP = 26 wt%	1.02	1. Sequential living anionic polymerization	pK_a = 4.98	Ref. 57
	PB-*b*-P2VP^{60}	M_n = 60 000 g mol^{-1} PB = 19 wt% P2VP = 81 wt%	1.03	1. Sequential living anionic polymerization 2. Core-crosslinking	pK_a = 4.98	Ref. 71 Ref. 72 Ref. 73
	PB-*b*-P2VP^{200}	M_n = 200 000 g mol^{-1} PB = 30 wt% P2VP = 70 wt%	Not reported	1. Sequential living anionic polymerization 2. Core-crosslinking	pK_a = 4.98	Ref. 74
Polybutadiene-*block*-poly(*N*-methyl-2-vinylpyridinium iodide), quaternized	PB-*b*-P2QVP$^+$	M_n = 60 000 g mol^{-1} PB = 19 wt% P2QVP$^+$ = 81 wt%	1.03	1. Sequential living anionic polymerization 2. Core-crosslinking 3. Methylation	pH independent (positive)	Ref. 75 Ref. 76
Poly(2-vinylpyridine)-*block*-poly(allyl methacrylate)	P2VP-*b*-PAMA	M_n = 74 000 g mol^{-1} P2VP = 75 wt% PAMA = 25 wt%	1.10	1. Sequential living anionic polymerization 2. Core-crosslinking	pK_a = 4.98	Ref. 77

[a] M_n = number average molecular weight. [b] Molar mass dispersity $Đ_M = M_w/M_n$. [c] pK_a values were taken from ref. 78 and 79.

amphiphilic diblock copolymers and oligo-anions require polar solvent such as water or tetrahydrofuran (THF), which would facilitate the formation of colloidal stable precursors. Furthermore, in order to realize thermally stable mesostructures the size of the inorganic precursors shall not exceed the root-mean-square end-to-end distance of the polyelectrolytic side chains.[66,67]

Based on this criteria, molecular inorganic oligo-ions and oxidic colloids carrying a surface charge have been identified as suitable inorganic precursor for the construction of mesostructured catalysts for thermal and photocatalytic processes.

The resulting mesomaterials, their chemistry and properties are described below. We first highlight results that were obtained by charged inorganic oligo-ions applying ROUTE 1 and ROUTE 2. These oligo-ions are mainly composed of Mo and W containing oxides. A special chapter is dedicated to the removal of the organic template from Mo containing mesostructures, thereby retaining the mesophase. This can be considered as non-trivial due to sublimation and gas phase sintering of Mo(VI) oxides. The second part of the examples is dedicated on results that have been obtained using colloidal stable precursors following ROUTE 2.

Example I. Charged inorganic oligo-ions

Polyoxometalates represent the most prominent oligo-ions that are characterized by distinct sizes, charges and shapes.[80,81] Due to their highly hydrophilic character they are difficult to be stabilized in hydrophobic polymeric matrices, which renders mesostructuring difficult. Nonetheless, the ELAN-strategy enables synthetic pathways toward mesostructured materials by grafting those charged inorganic molecular oligo-ions onto ionizable amphiphilic diblock copolymers, as has been shown for Keggin-type polyoxometalates.[57,69,70,74] These triply or quadruply charged oligo-anions have widespread applications in catalysis as well as electrochemistry and can act as strong inorganic acids.[82–85] Using the Keggin-type polyoxometalate $H_3[PMo_{12}O_{40}]$ as an example a synthetic protocol towards mesostructured polyoxometalates has been elaborated exploiting the EISA process (ROUTE 1).[69] This strong heteropoly acid can easily protonate the amino function of poly(*N*,*N*-dimethylaminoethyl methacrylate) (PDMAEMA, pK_a = 8.44) or the pyridine moiety of poly(2-vinypyridine) (P2VP, pK_a = 4.98).[78,79] The internal acid/base reaction would usually lead to an immediate precipitation of the inorganic/organic hybrid material. This is efficiently prevented by employing tailor-made amphiphilic diblock copolymers with a non-ionizable second block of sufficient length, providing solubility in organic solvents. Here, a long polybutadiene (PB) block was employed to prevent the precipitation of the PDMAEMA/Keggin-type polyoxometalate associate in THF as solvent. Cryogenic transmission electron microscopy (cryo-TEM) images (Fig. 2) of such homogeneous PB-*b*-PDMAEMA/Keggin-type polyoxometalate dispersions in THF disclose the presence of nanoobjects after combining inorganic and organic components. The structures of these nanoobjects strongly depend on the Keggin-type polyoxometalate loading as well as relative humidity and range from spherical micellar structures over bicontinuous networks to vesicles. In these nanoobjects the solvophobic core, which contains the Keggin-type polyoxometalates (dark), is shielded from the solvent by the solvophilic PB corona (bright). It has been found that clear solutions in combination with the initial occurrence of a

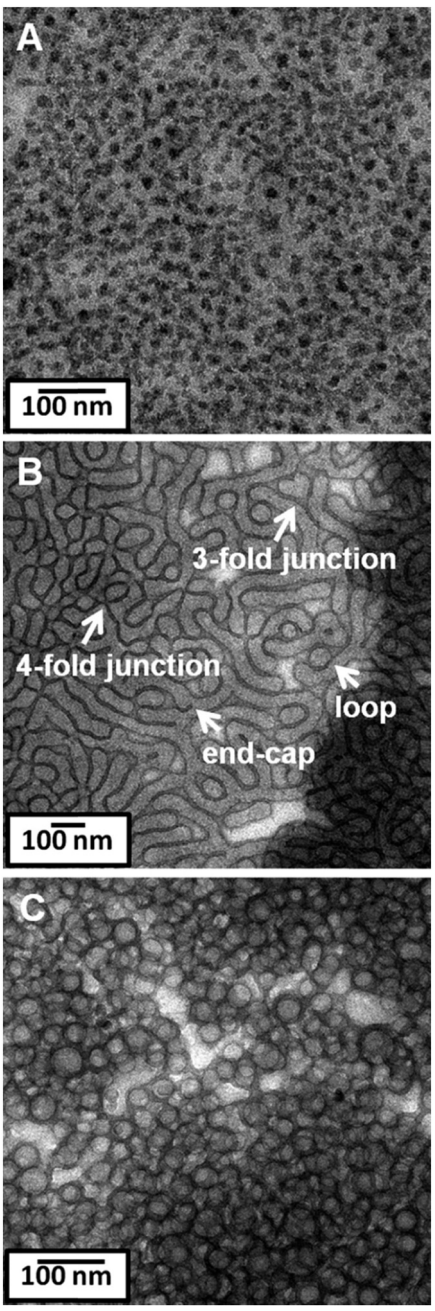

Fig. 2 Cryo-TEM images of PB-*b*-PDMAEMA/Keggin-type polyoxometalate nanostructures in THF with different PB-*b*-PDMAEMA/Keggin-type ratios: (A) 3.23, (B) 1.08, and (C) 0.54. Reprinted with permission from ref. 69. Copyright 2012 American Chemical Society.

bicontinuous network structure are pre-requisites for the formation of inverse hexagonally ordered PB-*b*-PDMAEMA/Keggin-type polyoxometalate mesostructures upon evaporation of the solvent at constant humidity. It shall be noted that this process allows for the formation of well-ordered organic/inorganic mesostructures with a unprecedented high Keggin-type polyoxometalate loading of around 70 wt%.

Mesostructured PB-*b*-P2VP/molybdophosphoric acid composites with an inverse hexagonally ordered structure can be converted *via* heat treatment at 740 °C under inert gas atmosphere into MoO_xC_y/C composites under retention of the mesostructure (Fig. 3). These mesostructured MoO_xC_y/C composites exhibit high surface areas and show a similar activity in the catalytic decomposition of ammonia as common molybdenum carbides.[57]

Although the above-mentioned approach can lead to well-ordered, catalytically active micro-/mesoporous functional materials, it is rather elaborate to yield the desired mesostructure as it is strongly influenced by micellar dynamics. For this particular example the dynamic nature of the *in situ* formed micelles seems to depend on the Keggin-type polyoxometalate loading, ionic strength or pH of the combined THF solution and even the relative humidity of the environment during evaporation. Moreover, it turned out that the hexagonal order of the mesopores has only little to no effect on the catalytic performance.[57]

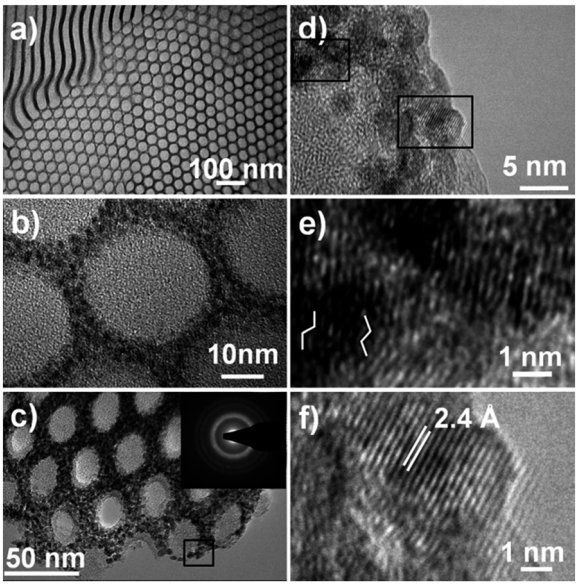

Fig. 3 Representative bright-field TEM images of PB-*b*-P2VP/Keggin-type polyoxometalate nanocomposites (a and b) and of MoO_xC_y/C at different magnifications (c–f). The inset in (c) represents a selected area electron diffraction (SAED) pattern indicative for nanocrystalline MoO_xC_y. d) Close-up of the area in the black box in (c). The black boxes in (d) denote selected areas of which HR-TEM images (e, top, and f, bottom) were taken. e) Displays the chevron-like structure of the vacancies of MoO_xC_y along the [010] zone axis. f) Shows a HR-TEM image of a single nanocrystal. The spacing of 0.24 nm is consistent with the (111) plane of MoO_xC_y. Reproduced from ref. 57 with permission from John Wiley and Sons.

The complexity related to micellar dynamics in the mesostructuring step can be eliminated by employing rigid, core-crosslinked cylindrical polymer brushes (CPB) with ionizable side chains (ROUTE 2 in Scheme 1) that can act as 1D template. An example for such a template is shown in Fig. 4: core-crosslinked CPBs with P2VP side chains based on a PB-*b*-P2VP diblock copolymer. These templates can be loaded with a heteropoly acid, *e.g.* tetravalent molybdosilicic acid ($H_4[SiMo_{12}O_{40}]$), which resulted in non-woven-like mesostructured PB-*b*-P2VP/Keggin-type polyoxometalate hybrid materials (Fig. 5). It is worth noting that during the incorporation of the Keggin-type polyoxometalate into the CPB template the 1D structure remains intact. These hybrid materials exhibit specific surface areas, which are almost ten times higher compared to the pristine heteropoly acid.[74] Such non-woven-like mesostructured CPB/Keggin-type polyoxometalate hybrid materials can be obtained with all kinds of Keggin-type polyoxometalate precursors as long as they are acidic. Furthermore their specific surface area is tuneable and depends on the length of the 1D CPB template and the packing of the dried mesostructured material (Fig. 6).[73]

Sonication for different times allows to adjust the length of the 1D CPB templates. After loading with $H_3[Mo_{12}PO_{40}]$ the specific surface area initially increases for low sonication time (1 min), which is followed by a steep decrease of the surface area for sonication times up to 2 min. Finally, longer sonication times lead to a steady increase of the surface area. As indicated by scanning electron microscopy (SEM) the change in surface area correlates to the different packing of the mesostructured 1D PB-*b*-P2VP CPB/Keggin-type polyoxometalate hybrid materials. Initially, the structure of the approximately parallel aligned cylindrical hybrid brushes breaks up and consequently more surface area is accessible. Next, shorter 1D CPB templates are produced by the ultrasound treatment that can realize a denser packing with significantly less accessible surface area. Finally, above 2 min sonication more and more approximately spherical particles are formed resulting in increasing surface areas.

When non-acidic oligo-anions are used as precursors, such as isopolyoxometalates, the 1D template first needs to be converted into a polycation by quaternization or by protonation with strong acids such as HCl: for instance, with

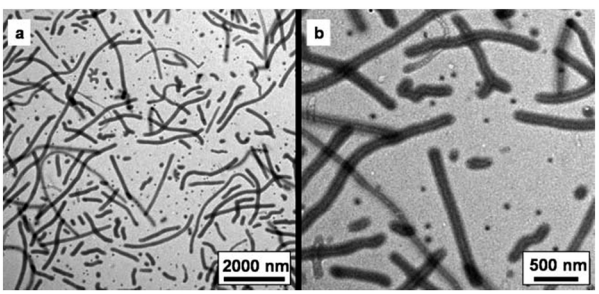

Fig. 4 Overview (a) and close up (b) TEM image of 1D core-crosslinked PB-*b*-P2VP CPB templates at different magnifications. Reproduced from ref. 74 with permission from The Royal Society of Chemistry.

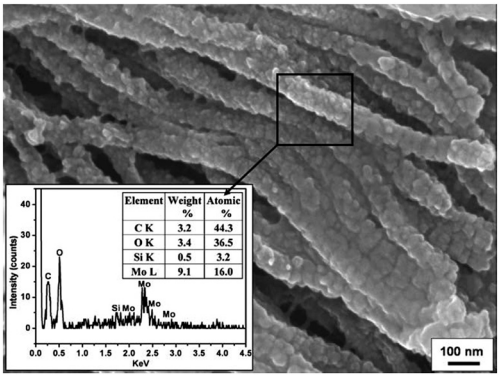

Fig. 5 SEM image of the $[SiMo_{12}O_{40}]^{4-}$ Keggin-type polyoxometalates grafted onto 1D core-crosslinked PB-*b*-P2VP CPB templates (inset: EDX spectrum). Reproduced from ref. 74 with permission from The Royal Society of Chemistry.

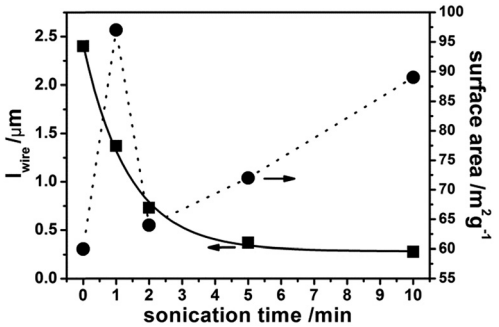

Fig. 6 Evolution of average CPB length (squares) and specific surface area of non-woven-like mesostructured PB-*b*-P2VP CPB/Keggin-type polyoxometalates (circles) as function of sonication time. Reproduced from ref. 73 with permission De Gruyter.

ammonium metatungstate ($(NH_4)_6H_2W_{12}O_{40}$) stable non-woven-like PB-*b*-PQ2VP$^+$ CPB/ammonium metatungstate mesostructures have been obtained that exhibit a specific surface area of 34 m^2 g^{-1}. After thermal template removal in oxidative atmosphere the mesostructure is preserved resulting in photocatalytic active tungsten oxide nanotubes. Owing to the density increase during crystallization of the walls the specific surface area of the WO_3 nanotubes decreased to 25 m^2 g^{-1}.[72] Most interestingly, due to the confinement, the walls of the nanotubes were constructed by a polycrystalline assembly of the metastable, orthorhombic polymorph of WO_3 which is stabilized by a crystallite nanosize effect.

Organic template removal

To exploit the full functionality of the initially obtained hybrid mesostructures, the polymeric template has to be removed. However, for molybdenum containing mesostructures this is by far not trivial. In systematic studies a large variety of different calcination and heat treatment conditions have been explored with similar outcome: the complete destruction of the mesostructure, which was accompanied by crystallization leading to the formation of coarse-grained MoO_3 crystals. Only harsh plasma edging on very thin, electron transparent films has resulted in stable mesoporous nanofilms (Fig. 7).[70]

The thermal instability can be attributed to the pronounced vapor pressure of MoO_3 above 400 °C that triggers fast gas phase sintering that in turn results in the formation of micrometre sized crystals. Of course, as a consequence, the mesostructure is destroyed. To work around the detrimental high sublimation rate of MoO_3 the oxidative removal of the template has to be conducted at an oxygen fugacity low enough to avoid the formation of Mo(VI). This requires a precise control of oxygen fugacity applying a buffer during template removal. As indicated by the Ellingham diagram (Fig. 8), carbonaceous material can be oxidized by CO_2 due to the Boudouard equilibrium, while this C/CO_2 buffer fixes the oxygen fugacity within the stability range of MoO_2. The vapor pressure of the latter is much lower than that of MoO_3, allowing for template removal and chemical transformations of the non-woven-like PB-*b*-P2VP CPB/dimolybdate while preserving the mesostructure. First, in inert atmosphere the hybrid material is converted into stable MoC/C composites. Then, as described above, the carbon is oxidized at buffered oxygen fugacity with CO_2 obtaining MoO_{2-x}. Finally, 1D MoO_{2-x} mesostructures can then be converted into MoO_3 or MoN nanowires, respectively. MoN nanowires exhibit an activation energy of 131 kJ mol^{-1} in the decomposition of ammonia.[71]

Alternatively to oxidative removal of the template, access to the internal mesopores of molybdenum oxide containing mesostructures can be obtained by thermal depolymerization of appropriate cores at temperatures below 400 °C. For instance, poly(allyl methacrylate) (PAMA) is a suitable candidate as it depolymerizes at temperatures around 280 °C.[77,86] Furthermore, the allyl moieties of PAMA can easily be crosslinked, which renders it also into a suitable candidate to form the core in rigid, 1D CPB templates. The resulting rigid 1D polymeric templates exhibit ionisable P2VP side chains and a PAMA core and can be dispersed in dilute aqueous HCl. Subsequent loading of pre-synthesized ammonium paramolybdate into the protonated P2VP/H$^+$ corona of the CPB template resulted in the formation of non-woven-like PAMA-*b*-P2VP CPB/ammonium paramolybdate mesostructures. After thermal treatment in vacuum the PAMA block was removed by depolymerisation. Then, the remaining amorphous P2VP/ammonium paramolybdate nanotubes were converted into MoC/C nanotubes with accessible internal surface area (Fig. 9).[77] In addition, the MoC/C nanotubes synthesized by this method exhibit an activation energy of 127 kJ mol^{-1} in the catalytic decomposition of ammonia, which is the lowest in the broad series of different MoC/C and MoN mesostructures.

Example II. Colloidal route

Silica mesostructures are redox-inert and electronically insulating and therefore typically serve as amorphous high surface area supports.[87–89] Contrary to this, for transition metal

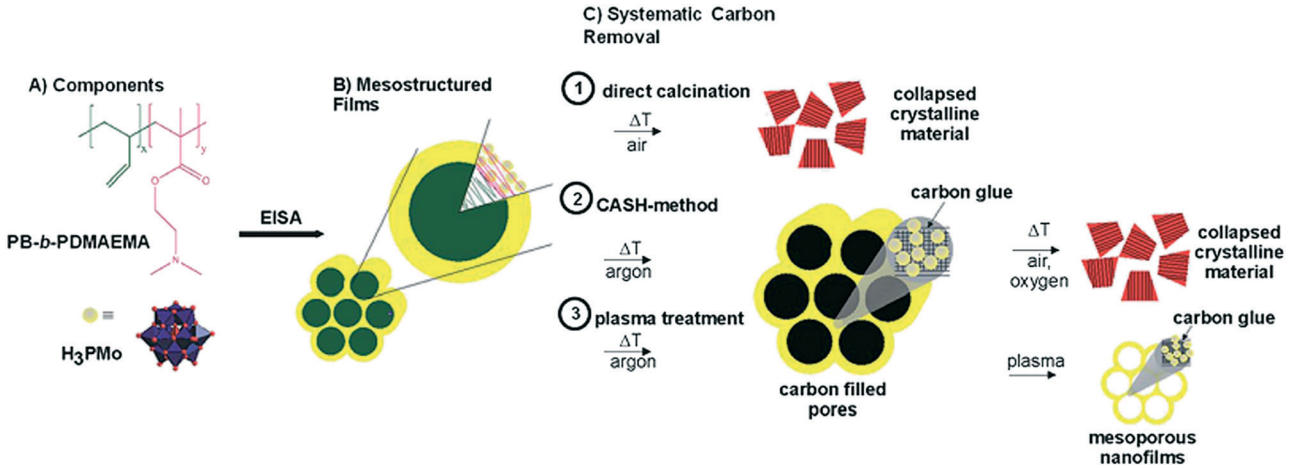

Fig. 7 (A) Structure of $H_3[Mo_{12}PO_{40}]$ and PB-*b*-PDMAEMA. *x* denotes the degree of polymerization (DP) of the PB block (*x* = 411), and *y* the DP of the PDMAEMA block (*y* = 40). (B) $H_3[PMo_{12}O_{40}]$ clusters were selectively incorporated into the PDMAEMA domains. (C) Systematic calcination studies were conducted either directly in air (1) or by applying a two-step heat treatment (2), *i.e.*, first in argon and second in an oxidative atmosphere. Alternatively, argon heat treated samples were exposed to H–O plasma (3). Reproduced from ref. 70 with permission from The Royal Society of Chemistry.

compounds the electronic structure is a key feature for their catalytic performance. Therefore, control of crystallinity and potentially polymorphism is crucial. Unfortunately, controlling these features upon mesostructuring of these materials is complicated, in particular, when 0 D molecular precursors are used. As already mentioned, with precursors like transition metal-alkoxides, hydrolysis and condensation is fast and typically amorphous materials are obtained during mesostructuring. Even with precursors that are stable with respect to further condensation, like the oligo-ions dealt with in the previous chapter, control of crystallinity and polymorphism while simultaneously self-assembling inorganic precursor and organic templates is difficult if not impossible. Crystallization requires high temperatures as experienced during template removal and, moreover, is strongly influenced by the confined space available in polymeric templates, which may act as nanoreactor dictating nucleation and growth.[68,72,86]

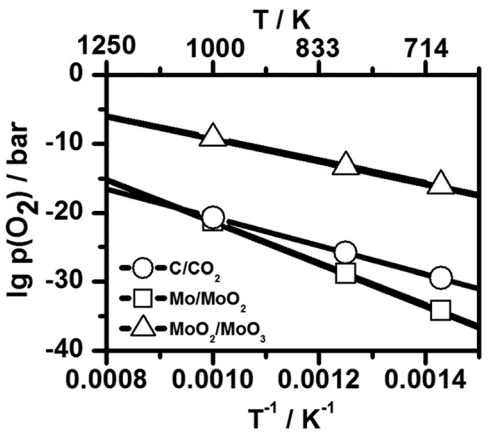

Fig. 8 Calculated Ellingham diagram for C/CO_2, Mo/MoO_2 and MoO_2/MoO_3 equilibrium lines. Adopted from ref. 71 with permission from John Wiley and Sons.

As an example, we will focus on the polymorphism of TiO_2. TiO_2 exhibits three main polymorphs (brookite, anatase, rutile). In the series of different polymorphs rutile is the thermodynamically most stable oxide. These polymorphs exhibit different electronic structures reflected in different physical properties such as refractive index, chemical reactivity and photocatalytic activity.[90,91] Thus, there is a strong need to have control over the crystal structure desired for specific applications. The crystal structure of the rutile polymorph is only rarely observed in mesostructured materials, as in the confined space of the polymeric template strong ligands have a strong affinity to the surface of TiO_2 and

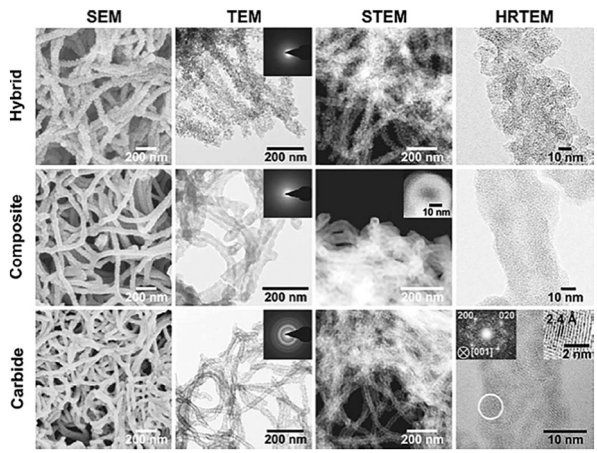

Fig. 9 SEM, TEM, STEM, and HRTEM images of non-woven-like PAMA-*b*-P2VP CPB/ammonium paramolybdate mesostructures, composite after thermal depolymerization in vacuum and MoO_xC_y nanotubes after carburization in argon atmosphere (inset in TEM column: SAED). The left inset in the HRTEM of the carbide denotes a power spectrum of the marked region of interest viewed along [001] of cubic MoO_xC_y. Reproduced from ref. 77 with permission from John Wiley and Sons.

promote the nucleation of anatase.[64] Attempts to thermally convert anatase mesostructures into rutile analogues often lead to the collapse of the mesostructure.

To master this polymorphism challenge, a two-step synthesis protocol has been established: (1) the synthesis of colloidally stable, nanoparticular inorganic precursors which exhibit charged surfaces, and (2) electrostatic grafting of these charged precursors onto the polyelectrolytic brushes of prestructured polymeric templates. This approach predetermines the polymorph already at the stage of the nanoparticulate inorganic precursor. Many synthesis protocols exist in literature that give access to desired polymorphic nanoparticles. Since CPB templates of varying pK_a values are available, resulting in both anionic and cationic functional groups, this colloidal route is most general and flexible. In addition, surface charges of the inorganic colloids are pre-determined by the point of zero charge (PZC). The PZC is determined by the basic or acidic nature of surface hydroxyl groups or surface capping agents. The degree of charged functional groups in CPB templates and the surface charges of inorganic colloids can be controlled by the pH value. Nanocrystalline TiO_2 in the rutile structure can for instance be obtained by HCl assisted sol–gel synthesis starting with titanium(IV) *n*-butoxide at pH < 1. The point of zero charge of titania is around 5. Thus, the obtained nanocrystalline rutile carries a positive surface charge. Mesostructuring requires an anionic group that even at pH ≈ 1 is still negatively charged. As opposed to sulfonate groups, carboxylate will therefore not work. Applying a spherical polyelectrolyte brush (SPB) consisting of a solid polystyrene core and a dense layer of surface-grafted poly(styrene sulfonate) allows for insertion of the preformed rutile nanocrystals into the polyelectrolyte brush. Calcination in air then resulted in photocatalytic active, porous rutile spheres.[91]

Moreover, the colloidal synthesis protocol is flexible enough to gain control over the polymorphism of TiO_2. While in HCl rutile is formed, the use of acetic acid as reaction medium results in nanoparticulate anatase. In this way, both high aspect ratio rutile and anatase nanowires could be prepared, employing for both polymorphic precursors the same 1D CPB template based on poly(styrene sulfonic acid)-*block*-poly(allyl methacrylate) (PSS-*b*-PAMA).[92]

ZnO is an important support in heterogeneous catalysis, it is photocatalytically active and exhibits a point of zero charge of around 9. Nanoparticulate ZnO can be stabilized by capping the surface with acetate, which in turn leads to a negative surface charge. Electrostatically driven, robust hybrid formation requires a positively charged CPB template, as provided by core-crosslinked PB-*b*-P2VP. By quaternization of the P2VP block with methyl iodide permanently positively charged brushes are generated. The incorporation of pre-synthesized, monodisperse ZnO nanocrystals into the positively charged corona of the CPB template resulted in high aspect ratio ZnO mesostructures. After thermal template removal the resulting ZnO nanotubes were highly active in the photocatalytic degradation of an anionic antibiotic under technically relevant conditions for hospital sewage treatment.[75] Using the same positively charged CPB template, 1D Au/ZnO heterostructures could be fabricated by co-mesostructuring of *in situ* generated Au nanoparticles and pre-formed ZnO nanoparticles. After thermal template removal the Au/ZnO mesostructures exhibit an enhanced photocatalytic activity as compared to neat ZnO nanotubes or commercial Degussa P25 (TiO_2) when applying the terrestrial solar spectra in the degradation of ciprofloxacin and levofloxacin, which are generic antibiotics frequently encountered in hospital sewage.[75] The improvement of the photocatalytic activity could be attributed to a better adsorption of the anionic antibiotics on the positively charged ZnO surfaces in the alkaline environment of hospital sewage. It may be additionally enhanced by the localized surface plasmon resonance effect of the Au nanoparticles.[76] The non-woven mesostructure, moreover, ensures easy recovery from the liquid reaction medium.

Besides the formation of non-woven transition oxides such as TiO_2 and ZnO, the ELAN-strategy can further also extended to SiO_2, which is an important support in heterogeneous catalysis.[88]

Conclusion

Employing Coulomb attraction between inorganic precursors and polymeric templates renders the ELAN-strategy most robust and versatile to obtain mesostructured hybrid materials. ELAN can of course be combined with various methods for removing the template while retaining the mesostructure and assuring a large accessible surface area. This includes more gentle and sophisticated methods, like depolymerization, oxidation at fixed oxygen fugacity employing an oxygen buffer like the Boudouard equilibrium, as well as the more established and harsher CASH method. The latter allows for high temperature annealing in various atmospheres under retention of the mesostructure. Together with the dimensional confinement in the wall CASH gives access to crystalline refractory catalysts including carbides and nitrides while preserving a high surface area due to slow Ostwald ripening. With ELAN polymorph control can be most easily implemented by employing pre-synthesized crystalline nanoparticulate precursors.

The mesostructured refractory catalysts have been tested in the thermal decomposition of ammonia and show similar activity than their bulk analogues, while the photocatalytic properties of mesostructured transition metal oxides seems to be enhanced compared to the corresponding bulk materials or industrial standards. Prospectively, the meso-immanent properties of mesostructured materials, such as lifetime enhancement, selectivity increase, or higher catalytic activity, need to be explored by systematic catalytic studies in order to conclude on the usefulness of this approach.

Conflicts of interest

There are no conflicts to declare.

Acknowledgements

This work has been generously supported by the German Science Foundation (DFG) within the collaborative research project SFB 840.

Notes and references

1 *Handbook of Heterogeneous Catalysis*, ed. G. Ertl, H. Knözinger, F. Schüth and J. Weitkamp, Wiley-VCH, Weinheim, 2nd edn, 2008.
2 R. J. White, R. Luque, V. L. Budarin, J. H. Clark and D. J. Macquarrie, *Chem. Soc. Rev.*, 2009, **38**, 481–494.
3 A. Kolmakov, D. O. Klenov, Y. Lilach, S. Stemmer and M. Moskovits, *Nano Lett.*, 2005, **5**, 667–673.
4 L. Masliuk, M. Heggen, J. Noack, F. Girgsdies, A. Trunschke, K. E. Hermann, M. G. Willinger, R. Schlögl and T. Lunkenbein, *J. Phys. Chem. C*, 2017, **121**, 24093–24103.
5 K. Mette, S. Kühl, A. Tarasov, M. G. Willinger, J. Kröhnert, S. Wrabetz, A. Trunschke, M. Scherzer, F. Girgsdies, H. Düdder, K. Kähler, K. F. Ortega, M. Muhler, R. Schlögl, M. Behrens and T. Lunkenbein, *ACS Catal.*, 2016, **6**, 7238–7248.
6 T. Lunkenbein, F. Girgsdies, T. Kandemir, N. Thomas, M. Behrens, R. Schlögl and E. Frei, *Angew. Chem., Int. Ed.*, 2016, **55**, 12708–12712.
7 T. Lunkenbein, J. Schumann, M. Behrens, R. Schlögl and M. G. Willinger, *Angew. Chem.*, 2015, **127**, 4627–4631.
8 C. Heine, M. Hävecker, M. Sanchez-Sanchez, A. Trunschke, R. Schlögl and M. Eichelbaum, *J. Phys. Chem. C*, 2013, **117**, 26988–26997.
9 G. Leofanti, M. Padovan, G. Tozzola and B. Venturelli, *Catal. Today*, 1998, **41**, 207–219.
10 D. R. Rolison, *Science*, 2003, **299**, 1698–1701.
11 X.-Y. Yang, L.-H. Chen, Y. Li, J. C. Rooke, C. Sanchez and B.-L. Su, *Chem. Soc. Rev.*, 2017, **46**, 481–558.
12 S. L. Suib, *Chem. Rec.*, 2017, **17**, 1169–1183.
13 J. Li, A. Corma and J. Yu, *Chem. Soc. Rev.*, 2015, **44**, 7112–7127.
14 M. Moliner, C. Martínez and A. Corma, *Angew. Chem., Int. Ed.*, 2015, **54**, 3560–3579.
15 K. S. W. Sing, *Pure Appl. Chem.*, 1985, **57**, 603–619.
16 Z.-Y. Yuan and B.-L. Su, *J. Mater. Chem.*, 2006, **16**, 663–677.
17 A. Taguchi and F. Schüth, *Microporous Mesoporous Mater.*, 2005, **77**, 1–45.
18 W. Li, J. Liu and D. Zhao, *Nat. Rev. Mater.*, 2016, **1**, 16023.
19 C. Sanchez, P. Belleville, M. Popall and L. Nicole, *Chem. Soc. Rev.*, 2011, **40**, 696–753.
20 X. Deng, K. Chen and H. Tüysüz, *Chem. Mater.*, 2017, **29**, 40–52.
21 Y. Xie, D. Kocaefe, C. Chen and Y. Kocaefe, *J. Nanomater.*, 2016, 1–10.
22 A. Thomas, F. Goettmann and M. Antonietti, *Chem. Mater.*, 2008, **20**, 738–755.
23 A. Huczko, *Appl. Phys. A: Mater. Sci. Process.*, 2000, **70**, 365–376.
24 H. Yang and D. Zhao, *J. Mater. Chem.*, 2005, **15**, 1217–1231.
25 N. Pal and A. Bhaumik, *Adv. Colloid Interface Sci.*, 2013, **189–190**, 21–41.
26 Y. Wan and Zhao, *Chem. Rev.*, 2007, **107**, 2821–2860.
27 W. Li and D. Zhao, *Chem. Commun.*, 2013, **49**, 943–946.
28 S. R. Quake and A. Scherer, *Science*, 2000, **290**, 1536–1540.
29 M.-P. Pileni, *Nat. Mater.*, 2003, **2**, 145–150.
30 X. W. Lou, L. A. Archer and Z. Yang, *Adv. Mater.*, 2008, **20**, 3987–4019.
31 Y. Liu, J. Goebl and Y. Yin, *Chem. Soc. Rev.*, 2013, **42**, 2610–2653.
32 C. G. Goltner and M. Antonietti, *Adv. Mater.*, 1997, **9**, 431–436.
33 J. Rodríguez-Hernández, F. Chécot, Y. Gnanou and S. Lecommandoux, *Prog. Polym. Sci.*, 2005, **30**, 691–724.
34 C. Sanchez, G. J. d. A. A. Soler-Illia, F. Ribot, T. Lalot, C. R. Mayer and V. Cabuil, *Chem. Mater.*, 2001, **13**, 3061–3083.
35 M. Zhang and A. H. E. Müller, *J. Polym. Sci., Part A: Polym. Chem.*, 2005, **43**, 3461–3481.
36 J. S. Beck, J. C. Vartuli, W. J. Roth, M. E. Leonowicz, C. T. Kresge, K. D. Schmitt, C. T. W. Chu, D. H. Olson, E. W. Sheppard, S. B. McCullen, J. B. Higgins and J. L. Schlenker, *J. Am. Chem. Soc.*, 1992, **114**, 10834–10843.
37 J. Y. Ying, C. P. Mehnert and M. S. Wong, *Angew. Chem., Int. Ed.*, 1999, **38**, 56–77.
38 D. Zhao, J. Feng, Q. Huo, N. Melosh, G. H. Fredrickson, B. F. Chmelka and G. D. Stucky, *Science*, 1998, **279**, 548–552.
39 S. L. Wang, H. Xu, L. Q. Qian, X. Jia, J. W. Wang, Y. Y. Liu and W. H. Tang, *J. Solid State Chem.*, 2009, **182**, 1088–1093.
40 G. Q. Liu, Z. G. Jin, X. X. Liu, T. Wang and Z. F. Liu, *J. Sol-Gel Sci. Technol.*, 2007, **41**, 49–55.
41 T. S. Atabaev, J. H. Lee, J. J. Lee, D. W. Han, Y. H. Hwang, H. K. Kim and N. H. Hong, *Nanotechnology*, 2013, **24**, 345603.
42 V. Malgras, Q. Ji, Y. Kamachi, T. Mori, F.-K. Shieh, K. C.-W. Wu, K. Ariga and Y. Yamauchi, *Bull. Chem. Soc. Jpn.*, 2015, **88**, 1171–1200.
43 B. Smarsly and M. Antonietti, *Eur. J. Inorg. Chem.*, 2006, **2006**, 1111–1119.
44 D. Gu and F. Schuth, *Chem. Soc. Rev.*, 2014, **43**, 313–344.
45 J. Livage, M. Henry and C. Sanchez, *Prog. Solid State Chem.*, 1988, **18**, 259–341.
46 Y. Xia, P. Yang, Y. Sun, Y. Wu, B. Mayers, B. Gates, Y. Yin, F. Kim and H. Yan, *Adv. Mater.*, 2003, **15**, 353–389.
47 C. J. Brinker, Y. Lu, A. Sellinger and H. Fan, *Adv. Mater.*, 1999, **11**, 579–585.
48 C. Sanchez and M. In, *J. Non-Cryst. Solids*, 1992, **147–148**, 1–12.
49 U. Schubert, N. Huesing and A. Lorenz, *Chem. Mater.*, 1995, **7**, 2010–2027.
50 G. J. d. A. A. Soler-Illia, C. Sanchez, B. Lebeau and J. Patarin, *Chem. Rev.*, 2002, **102**, 4093–4138.
51 W. Li, Q. Yue, Y. Deng and D. Zhao, *Adv. Mater.*, 2013, **25**, 5129–5152.
52 F. Schüth, *Angew. Chem.*, 2003, **115**, 3730–3750.
53 T. J. Barton, L. M. Bull, W. G. Klemperer, D. A. Loy, B. McEnaney, M. Misono, P. A. Monson, G. Pez, G. W. Scherer, J. C. Vartuli and O. M. Yaghi, *Chem. Mater.*, 1999, **11**, 2633–2656.

54 M. C. Orilall and U. Wiesner, *Chem. Soc. Rev.*, 2011, **40**, 520–535.
55 J. Lee, M. Christopher Orilall, S. C. Warren, M. Kamperman, F. J. DiSalvo and U. Wiesner, *Nat. Mater.*, 2008, **7**, 222–228.
56 T. Katou, B. Lee, D. Lu, J. N. Kondo, M. Hara and K. Domen, *Angew. Chem., Int. Ed.*, 2003, **42**, 2382–2385.
57 T. Lunkenbein, D. Rosenthal, T. Otremba, F. Girgsdies, Z. Li, H. Sai, C. Bojer, G. Auffermann, U. Wiesner and J. Breu, *Angew. Chem., Int. Ed.*, 2012, **51**, 12892–12896.
58 J. Y. Cheng, C. A. Ross, H. I. Smith and E. L. Thomas, *Adv. Mater.*, 2006, **18**, 2505–2521.
59 J. Yuan and A. H. E. Müller, *Polymer*, 2010, **51**, 4015–4036.
60 Y. Deng, J. Wei, Z. Sun and D. Zhao, *Chem. Soc. Rev.*, 2013, **42**, 4054–4070.
61 K. Koo, H. Ahn, S.-W. Kim, D. Y. Ryu and T. P. Russell, *Soft Matter*, 2013, **9**, 9059–9071.
62 S. Förster and M. Antonietti, *Adv. Mater.*, 1998, **10**, 195–217.
63 X. Guo, A. Weiss and M. Ballauff, *Macromolecules*, 1999, **32**, 6043–6046.
64 Y. Lu, A. Wittemann and M. Ballauff, *Macromol. Rapid Commun.*, 2009, **30**, 806–815.
65 A. Walther, A. S. Goldmann, R. S. Yelamanchili, M. Drechsler, H. Schmalz, A. Eisenberg and A. H. E. Müller, *Macromolecules*, 2008, **41**, 3254–3260.
66 S. C. Warren, F. J. DiSalvo and U. Wiesner, *Nat. Mater.*, 2007, **6**, 156–161.
67 S. C. Warren, L. C. Messina, L. S. Slaughter, M. Kamperman, Q. Zhou, S. M. Gruner, F. J. DiSalvo and U. Wiesner, *Science*, 2008, **320**, 1748–1752.
68 M. Müllner, T. Lunkenbein, N. Miyajima, J. Breu and A. H. E. Müller, *Small*, 2012, **8**, 2636–2640.
69 T. Lunkenbein, M. Kamperman, Z. Li, C. Bojer, M. Drechsler, S. Förster, U. Wiesner, A. H. E. Müller and J. Breu, *J. Am. Chem. Soc.*, 2012, **134**, 12685–12692.
70 T. Lunkenbein, M. Kamperman, M. Schieder, S. With, Z. Li, H. Sai, S. Forster, U. Wiesner and J. Breu, *J. Mater. Chem. A*, 2013, **1**, 6238–6248.
71 M. Schieder, C. Bojer, J. vom Stein, S. Koch, T. Martin, H. Schmalz, J. Breu and T. Lunkenbein, *Angew. Chem.*, 2017, **129**, 14156–14160 (*Angew. Chem. Int. Ed.*, 2017, **56**, 13968–13972).
72 M. Schieder, T. Lunkenbein, T. Martin, W. Milius, G. Auffermann and J. Breu, *J. Mater. Chem. A*, 2013, **1**, 381–387.
73 T. Lunkenbein, M. Schieder, C. Bojer, A. H. Müller and J. Breu, *Z. Phys. Chem.*, 2012, **226**, 815–826.
74 R. S. Yelamanchili, A. Walther, A. H. E. Müller and J. Breu, *Chem. Commun.*, 2008, 489–491.
75 C. Bojer, J. Schöbel, T. Martin, M. Ertl, H. Schmalz and J. Breu, *Appl. Catal., B*, 2017, **204**, 561–565.
76 C. Bojer, J. Schöbel, T. Martin, T. Lunkenbein, D. R. Wagner, A. Greiner, J. Breu and H. Schmalz, *Polymer*, 2017, **128**, 65–70.
77 M. Schieder, T. Lunkenbein, C. Bojer, M. Dulle, J. vom Stein, G. Auffermann, T. Löbling, J. Schöbel, H. Schmalz and J. Breu, *Z. Anorg. Allg. Chem.*, 2015, **641**, 1829–1834.
78 P. van de Wetering, E. E. Moret, N. M. E. Schuurmans-Nieuwenbroek, M. J. van Steenbergen and W. E. Hennink, *Bioconjugate Chem.*, 1999, **10**, 589–597.
79 K. Paek, H. Yang, J. Lee, J. Park and B. J. Kim, *ACS Nano*, 2014, **8**, 2848–2856.
80 M. T. Pope and A. Müller, *Polyoxometalate Chemistry From Topology via Self-Assembly to Applications*, Springer, Netherlands, 2007.
81 M. T. Pope, *Heteropoly and isopoly oxometalates*, Springer-Verlag, 1983.
82 M. Hashimoto, K. Itoh, K. Lee and M. Misono, *Top. Catal.*, 2001, **15**, 265–271.
83 I. V. Kozhevnikov, *Chem. Rev.*, 1998, **98**, 171–198.
84 I. V. Kozhevnikov, *Catal. Rev.: Sci. Eng.*, 1995, **37**, 311–352.
85 M. Misono, N. Mizuno, H.-o. Mori, K. Y. Lee, J. Jiao and T. Okuhara, *Stud. Surf. Sci. Catal.*, ed. R. K. Grasselli and A. W. Sleight, Elsevier, 1991, vol. 67, pp. 87–97.
86 S. Zulfiqar, A. Piracha and K. Masud, *Polym. Degrad. Stab.*, 1996, **52**, 89–93.
87 K. Amakawa, L. Sun, C. Guo, M. Hävecker, P. Kube, I. E. Wachs, S. Lwin, A. I. Frenkel, A. Patlolla, K. Hermann, R. Schlögl and A. Trunschke, *Angew. Chem., Int. Ed.*, 2013, **52**, 13553–13557.
88 M. Müllner, T. Lunkenbein, J. Breu, F. Caruso and A. H. E. Müller, *Chem. Mater.*, 2012, **24**, 1802–1810.
89 M. Müllner, J. Yuan, S. Weiss, A. Walther, M. Förtsch, M. Drechsler and A. H. E. Müller, *J. Am. Chem. Soc.*, 2010, **132**, 16587–16592.
90 M. Zhang, T. Chen and Y. Wang, *RSC Adv.*, 2017, **7**, 52755–52761.
91 R. S. Yelamanchili, Y. Lu, T. Lunkenbein, N. Miyajima, L.-T. Yan, M. Ballauff and J. Breu, *Small*, 2009, **5**, 1326–1333.
92 M. Müllner, T. Lunkenbein, N. Miyajima, J. Breu and A. H. E. Müller, *Small*, 2012, **8**, 2636–2640.

